Acoustic Wavefield Imaging Course

Ana Ramírez and Sergio Abreo

Universidad Industrial de Santander

CPS RESEARCH GROUP

Universidad Industrial de Santander

February 17-21, 2025

Connectivity and Signal Processing Research Group.
info@cps.uis.edu.co https://cpsuis.wordpress.com

Agenda

Introduction

Some previous work on AI for signal processing

- Generative Adversarial Networks (GAN) to improve spatial resolution in inverted velocity fields [Flórez et al., 2020]. **Seismic**.
- First arrival detection of seismological data from the Middle Magdalena Valley in Colombia using a cGAN [Abreo et al., 2023]. **Seismological**.
- System based on generative adversarial neural networks (GAN) for obtaining acoustic seismograms from elastic seismograms [Ramírez et al., 2024]. **Seismic**.
- Automatic first-break picking in seismic data with characteristics of the Middle Magdalena Valley in Colombia [Rincón et al., 2024]. **Seismological**.
- Physics-Informed Neural Network for the Seismic Velocity Problem using Neural Tangent Kernels [López et al., 2024]. **Seismological**.
- Design of a Synthetic Breast Ultrasound Image Database [Solano et al., 2024]. **Medical**.
- Physics-Informed Neural Network for the Inverse Seismic Problem using Neural Tangent Kernels [Bohórquez et al., 2024]. **Seismological**.

Introduction

Generative Adversarial Networks (GAN) to improve spatial resolution in inverted velocity fields [Flórez et al., 2020]. **Seismic**.

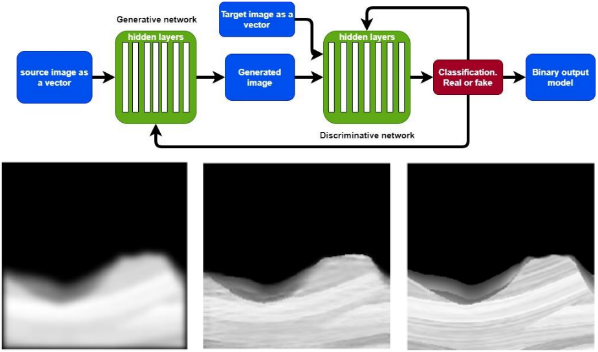

Figure 1: GAN and results.

Introduction

First arrival detection of seismological data from the Middle Magdalena Valley in Colombia using a cGAN [Abreo et al., 2023]. **Seismological**

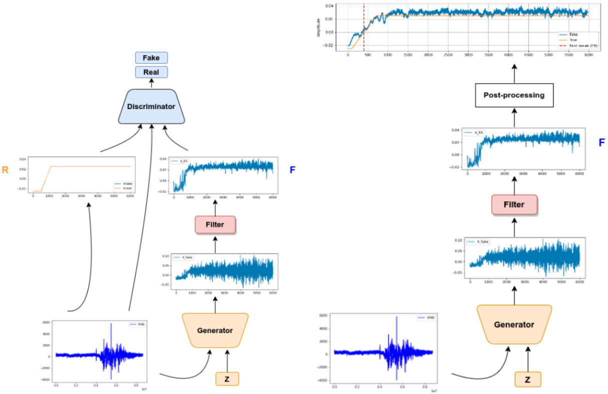

Figure 2: GAN and generator.

Introduction

System based on generative adversarial neural networks (GAN) for obtaining acoustic seismograms from elastic seismograms [Ramírez et al., 2024]. **Seismic**

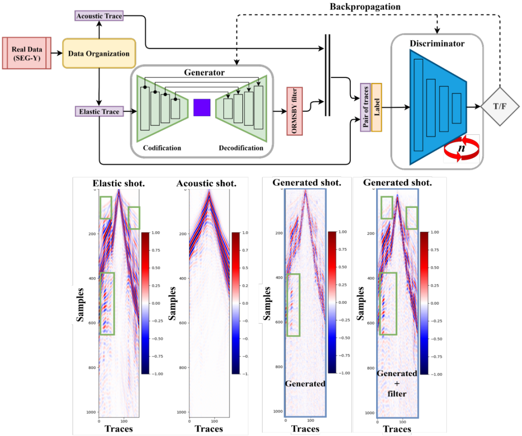

Figure 3: GAN and results.

Introduction

Physics-Informed Neural Network for the Seismic Velocity Problem using Neural Tangent Kernels [López et al., 2024]. **Seismological**.

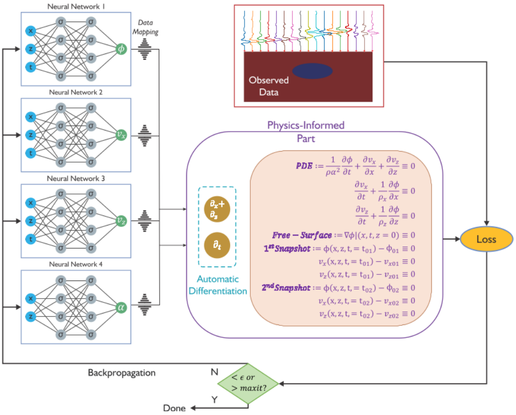

Figure 4: Proposed PINN.

PINN for forward and inverse problems

Schematics of PINNs' workflow

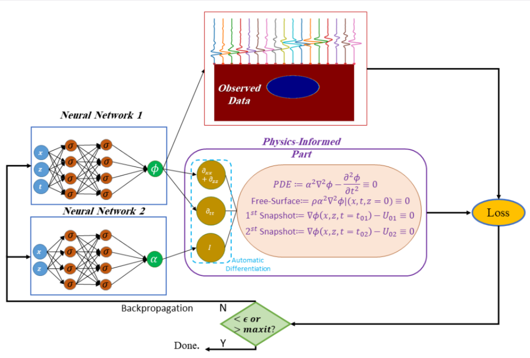

Figure 5: Left: Fully connected feed-forward neural network, the output of which approximates the solution to the forward and inverse problems. Right: The governing physical laws and the observed real-world data, i.e., seismograms, used to optimize the parameters of the PINN. The training stops when the loss error becomes smaller than a threshold, or the number of iterations goes beyond a set value.

PINN+FWI

Physics-Informed Neural Networks (PINNs) for Wave Propagation and Full Waveform Inversions

- [Rasht-Behesht et al., 2022] present the first FWI for seismological applications using PINNs.
- In this study, they focus on the development of acoustic FWI with PINNs and demonstrate its practical application to various synthetic case studies.

The salient results of their study are:

- In most applications of PINNs, authors have incorporated training data sets from within the computational domain from other solvers or experimental data, which greatly facilitates the training process.
- In contrast, with seismic inversions, this is generally not possible (records of the wavefield are generally limited spatially to the surface or boreholes).
- [Rasht-Behesht et al., 2022] show that this limitation does not prevent PINNs from performing efficient and accurate seismic inversions.

Neural Network

NN of [Rasht-Behesht et al., 2022]

- In the absence of any justifiable reasons to do otherwise, they, define a fully connected feed-forward NN with an input layer consisting of the physical coordinates x, z and time t, L hidden layers and an output layer representing the scalar acoustic wave potential $\phi \subset \mathbb{R}$.
- The various other physical variables, such as displacement or pressure, are obtained through the automatic differentiation of the wave potential NN using TensorFlow.
- The network's parameters are initialized from independent and identically distributed (iid) samples.
- They choose $\sigma = tanh(\cdot)$ *or* $sin(\cdot)$ as the nonlinear activation function for all NNs.
- They follow PINNs' original framework [Raissi et al., 2019], to obtain the parameters of a NN such that it closely approximates the acoustic wave potential ϕ.

$$\alpha^2 \nabla^2 \phi + f = \frac{\partial^2 \phi}{\partial t^2} \tag{1}$$

$$\alpha = \sqrt{\frac{k}{\rho}} \tag{2}$$

PINN for forward problem

Residual terms

- The observed data in the form of synthetic seismograms and the early-time snapshots are obtained from SpecFem2D simulations [Tromp et al., 2008], [Komatitsch and Tromp, 1999] a spectral element model for solving the wave equations in elastic/acoustic media.

$R_{PDE} \coloneqq \alpha^2 \nabla^2 \phi - \frac{\partial^2 \phi}{\partial t^2}$	PDE
$R_{P.C} \coloneqq \rho \alpha^2 \nabla^2 \phi(x, t, z = 0)$	Free-Surface Constraint
$R_{S_1} \coloneqq \nabla \phi(x, z, t = t_1^0) - \overrightarrow{U_1^0}(x, z)$	First time-snapshot
$R_{S_2} \coloneqq \nabla \phi(x, z, t = t_2^0) - \overrightarrow{U_2^0}(x, z)$	Second time-snapshot
$R_{obs} \coloneqq \nabla \phi(x, z, t) - \overrightarrow{U_{obs}}(x, z, t)$	Observed data (For inversions)

Figure 6: Aim to minimize.

PINN for forward problem

Schematic representation of a hypothetical computational domain (x, z and t) with PINN

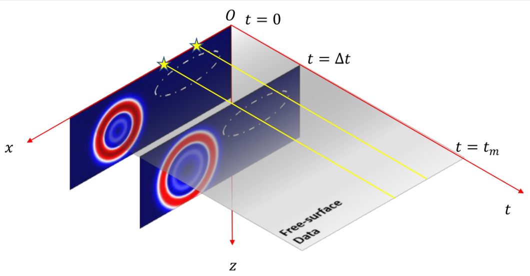

Figure 7: The two time-snapshots at times 0 and Δt are the only labeled data used from within the computational domain. The time-snapshots are color-coded for displacement amplitude. The white dashed line encloses a hypothetical heterogeneity. The grey hyperplane represents domain where the training data to apply, for example, a free-surface condition at the top of the domain. The two yellow stars represent the position of seismometers. t_m is the duration of the time domain. The PDE training data is selected randomly from the entire computational domain.

PINN for forward problem

The objective of the training process is to minimize the sum of mean squared errors

$$MSE(\Theta) = \lambda_1 MSE_{PDE} + \lambda_2 MSE_S + \lambda_3 MSE_{P.C.} + \lambda_4 MSE_{Obs} \quad (3)$$

loss term corresponding to the wave equation evaluated on a set of N_{PDE} randomly chosen PDE training data $(x_i, z_i, t_i) \subset \Omega$ with $\Omega = \mathbb{R}^2 \; x \; \mathbb{R}$

$$MSE_{PDE} = \frac{1}{N_{PDE}} \sum_{i=1}^{N_{PDE}} |R_{PDE}(x_i, z_i, t_i)|^2 \quad (4)$$

loss term corresponding to the two vectorial early-time snapshot data $\overrightarrow{U_1^0}$ and $\overrightarrow{U_2^0}$ in terms of displacement

$$MSE_S = \frac{1}{N_{S_1}} \sum_{i=1}^{N_{S_1}} |R_{S1}(x_i, z_i, t_i = t_1^0)|^2 + \frac{1}{N_{S_2}} \sum_{i=1}^{N_{S_2}} |R_{S2}(x_i, z_i, t_i = t_2^0)|^2 \quad (5)$$

PINN for forward problem

loss term corresponding to free surface constraint

$$MSE_{P.C.} = \frac{1}{N_{P.C.}} \sum_{i=1}^{N_{P.C.}} |R_{P.C.}(x_i, z_i, t_i)|^2 \tag{6}$$

loss term corresponding to the observed data

$$MSE_{Obs} = \frac{1}{N_{Obs}} \sum_{i=1}^{N_{Obs}} |R_{Obs}(x_i, z_i, t_i)|^2 \tag{7}$$

hyperparameters

- The hyperparameters are set to $\lambda_1 = \lambda_3 = 0.1$; $\lambda_2 = \lambda_4 = 1$.
- They found the proper values of $\lambda_{i,s}$ heuristically from trial and error.
- [Wang et al., 2021] proposed utilizes gradient statistics during the training process that would help maintaining a balance between different loss terms.

Results Case 3, Crosswell experiment

PoC: Ellipsoidal velocity anomaly with a single point source.

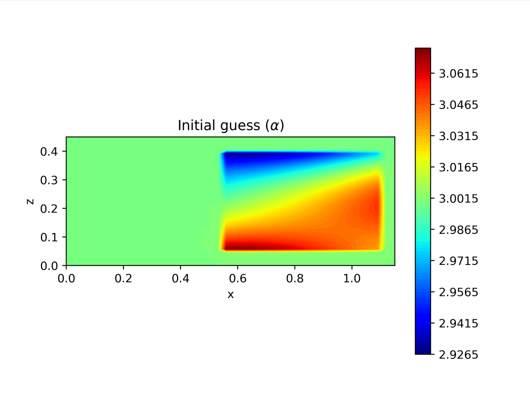

Figure 8: Initial velocity model.

Results Case 3, Crosswell experiment

PoC: Ellipsoidal velocity anomaly with a single point source.

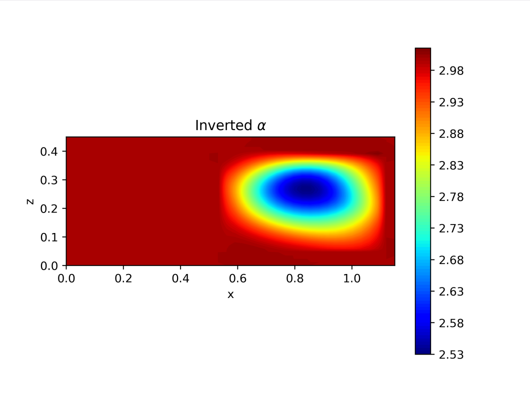

Figure 9: Final velocity model.

Results Case 3, Crosswell experiment

PoC: Ellipsoidal velocity anomaly with a single point source.

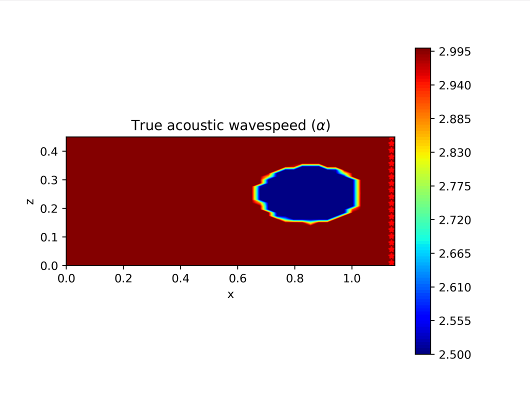

Figure 10: True velocity model.

Results Case 3, Crosswell experiment

PoC: Ellipsoidal velocity anomaly with a single point source.

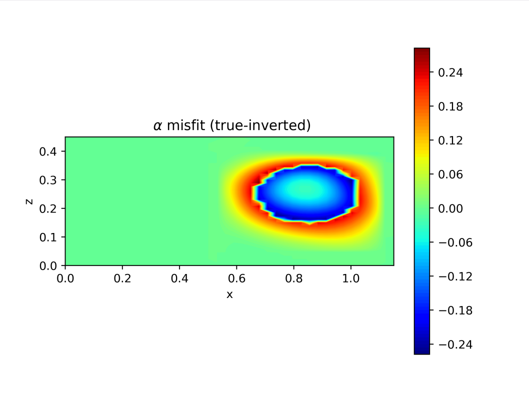

Figure 11: Velocity misfit.

Results Case 3, Crosswell experiment

PoC: Ellipsoidal velocity anomaly with a single point source.

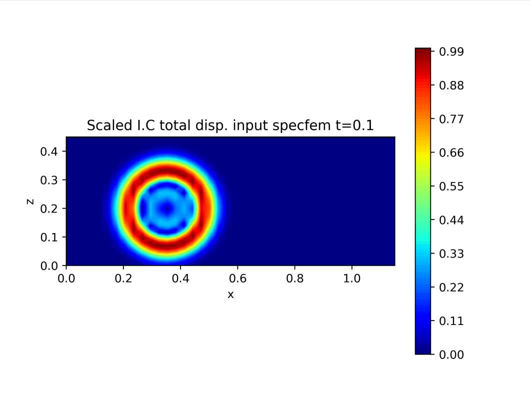

Figure 12: SpecFem snap 01.

Results Case 3, Crosswell experiment

PoC: Ellipsoidal velocity anomaly with a single point source.

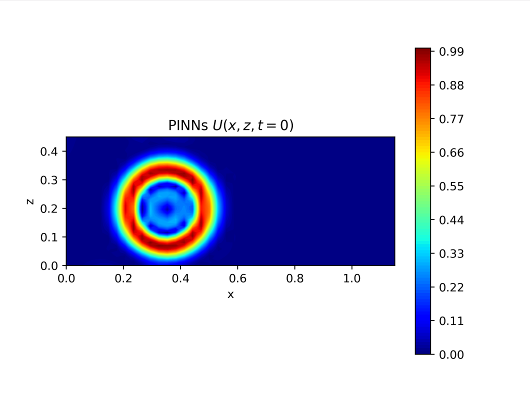

Figure 13: PINN snap 01.

Results Case 3, Crosswell experiment

PoC: Ellipsoidal velocity anomaly with a single point source.

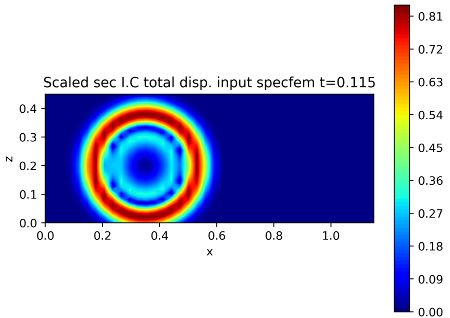

Figure 14: SpecFem snap 02.

Results Case 3, Crosswell experiment

PoC: Ellipsoidal velocity anomaly with a single point source.

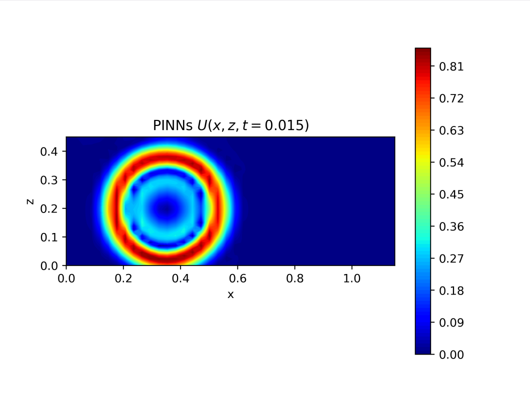

Figure 15: PINN snap 02.

Results Case 3, Crosswell experiment

PoC: Ellipsoidal velocity anomaly with a single point source.

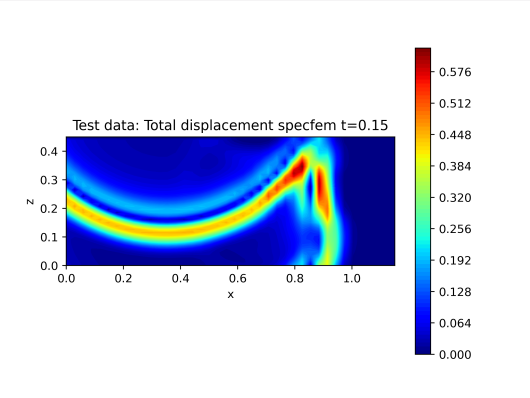

Figure 16: SpecFem snap 03.

Results Case 3, Crosswell experiment

PoC: Ellipsoidal velocity anomaly with a single point source.

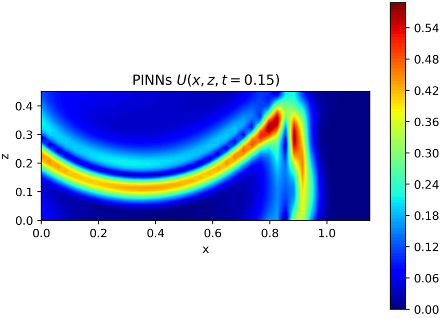

Figure 17: PINN snap 03.

Results Case 3, Crosswell experiment

PoC: Ellipsoidal velocity anomaly with a single point source.

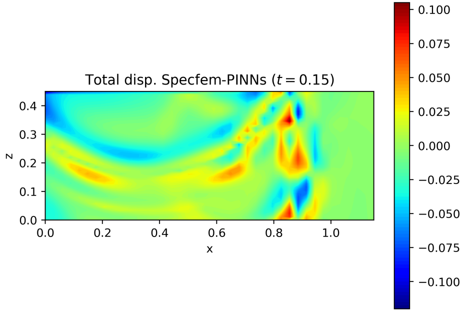

Figure 18: Snap 03 difference.

Results Case 3, Crosswell experiment

PoC: Ellipsoidal velocity anomaly with a single point source.

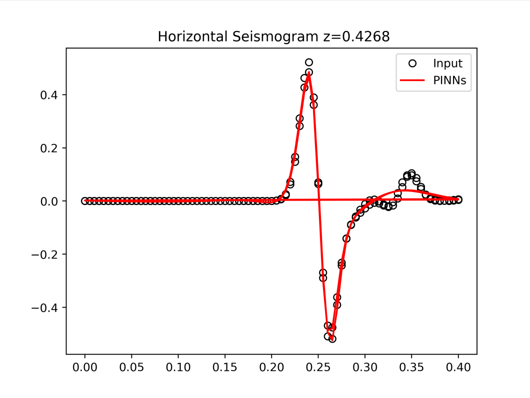

Figure 19: X-direction movement.

Results Case 3, Crosswell experiment

PoC: Ellipsoidal velocity anomaly with a single point source.

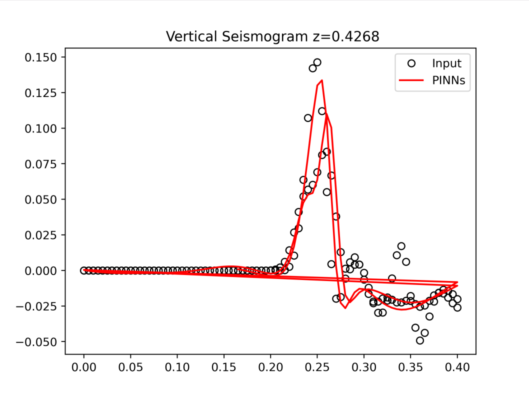

Figure 20: Z-direction movement.

Results Case 3, Crosswell experiment

PoC: Ellipsoidal velocity anomaly with a single point source.

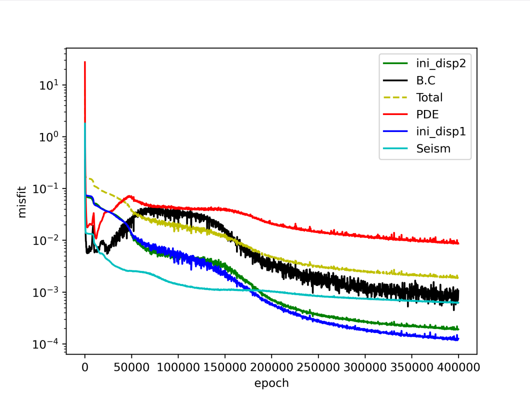

Figure 21: Loss function evolution.

[Rasht-Behesht et al., 2022] recommendations.

- The number of inputs/outputs of the neural network defines the standard deviation of its weights, assuming normal sampling, to improve the optimization process [Glorot and Bengio, 2010].
- The domain sampling is based on the sobol sequence [Sobol', 1967].
- The two neural network definitions can be taken from [Raissi et al., 2019].
- In their experiments, [Raissi et al., 2019] test the number of layers, the number of neurons, the number of points for training, among others parameters.

Random sampling.

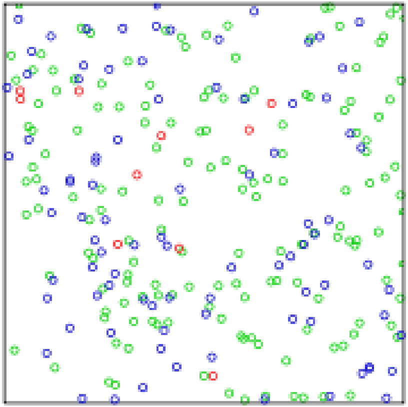

Table 1: Spatial distribution of 256 points.

Sobol sampling.

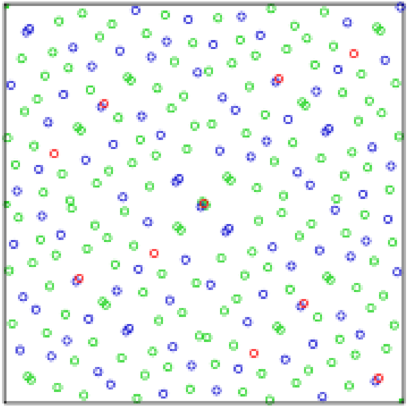

Table 2: Spatial distribution of 256 points.

PINNfwi Conda environment

```
conda create --name PINNfwi
conda activate PINNfwi
conda install python=3.7
conda install keras
conda install tensorflow
conda install tensorflow-gpu # para usar las GPUs del cluster
pip install salib
conda deactivate
```

Figure 22: Creating PINNfwi environment.

```
conda activate PINNfwi
python PINNs_Inversion_Acoustic.oy
conda deactivate
```

Figure 23: Using PINNfwi environment.

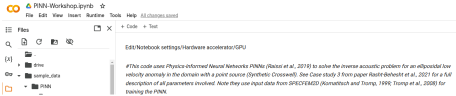

Figure 24: PINN-Workshop.

References I

Abreo, S., Reyes, O., Ramírez, A., and Serrano, J. (2023).
First arrival detection of seismological data from the middle magdalena valley in colombia using a cgan.
In *84th EAGE Annual Conference & Exhibition*, volume 2023, pages 1–5. European Association of Geoscientists & Engineers.

Bohórquez, J., Abreo, S., Ramírez, A., and Gil, S. (2024).
Physics-informed neural network for the inverse seismic problem using neural tangent kernels.
In *First EAGE Workshop on The Role of AI in FWI*, volume 2024, pages 1–6. European Association of Geoscientists & Engineers.

Flórez, A., Abreo, S., and Reyes, O. (2020).
Generative adversarial networks (gan) to improve spatial resolution in inverted velocity fields.
In *First EAGE Conference on Machine Learning in Americas*, volume 2020, pages 1–5. European Association of Geoscientists & Engineers.

Glorot, X. and Bengio, Y. (2010).
Understanding the difficulty of training deep feedforward neural networks.
In *Proceedings of the thirteenth international conference on artificial intelligence and statistics*, pages 249–256. JMLR Workshop and Conference Proceedings.

Komatitsch, D. and Tromp, J. (1999).
Introduction to the spectral element method for three-dimensional seismic wave propagation.
Geophysical journal international, 139(3):806–822.

References II

López, J. B., Silva, A. R., and Abreo, S. (2024).
Physics-informed neural network for the seismic velocity problem using neural tangent kernels.
In *Fourth EAGE Digitalization Conference & Exhibition*, volume 2024, pages 1–5. European Association of Geoscientists & Engineers.

Raissi, M., Perdikaris, P., and Karniadakis, G. E. (2019).
Physics-informed neural networks: A deep learning framework for solving forward and inverse problems involving nonlinear partial differential equations.
Journal of Computational physics, 378:686–707.

Ramírez, D., Abreo, S., Reyes, O., and Ramírez, A. (2024).
System based on generative adversarial neural networks (gan) for obtaining acoustic seismograms from elastic seismograms.
In *Fourth EAGE Digitalization Conference & Exhibition*, volume 2024, pages 1–5. European Association of Geoscientists & Engineers.

Rasht-Behesht, M., Huber, C., Shukla, K., and Karniadakis, G. E. (2022).
Physics-informed neural networks (pinns) for wave propagation and full waveform inversions.
Journal of Geophysical Research: Solid Earth, 127(5):e2021JB023120.

Rincón, S., Reyes, O., Abreo, S., and Ramírez, A. (2024).
Automatic first-break picking in seismic data with characteristics of the middle magdalena valley in colombia.
In *Fourth EAGE Digitalization Conference & Exhibition*, volume 2024, pages 1–5. European Association of Geoscientists & Engineers.

References III

Sobol', I. M. (1967).
On the distribution of points in a cube and the approximate evaluation of integrals.
Zhurnal Vychislitel'noi Matematiki i Matematicheskoi Fiziki, 7(4):784–802.

Solano, J. C., Ramirez, A. B., and Abreo, S. A. (2024).
Design of a synthetic breast ultrasound image database.
In *2024 IEEE UFFC Latin America Ultrasonics Symposium (LAUS)*, pages 1–4. IEEE.

Tromp, J., Komatitsch, D., and Liu, Q. (2008).
Spectral-element and adjoint methods in seismology.
Communications in Computational Physics, 3(1):1–32.

Wang, S., Teng, Y., and Perdikaris, P. (2021).
Understanding and mitigating gradient flow pathologies in physics-informed neural networks.
SIAM Journal on Scientific Computing, 43(5):A3055–A3081.